frontiers | Frontiers in Earth Science

TYPE Original Research
PUBLISHED 26 November 2025
DOI 10.3389/feart.2025.1719687

OPEN ACCESS

EDITED BY
James D. Muirhead,
The University of Auckland, New Zealand

REVIEWED BY
Páll Einarsson,
University of Iceland, Iceland
Stefano Urbani,
Istituto Superiore per la Protezione e la Ricerca Ambientale (ISPRA), Italy

*CORRESPONDENCE
Alessandro La Rosa,
alessandro.larosa@dst.unipi.it

RECEIVED 06 October 2025
REVISED 10 November 2025
ACCEPTED 13 November 2025
PUBLISHED 26 November 2025

CITATION
La Rosa A, Pagli C, Keir D, Ayele A, Wang H, Rivalta E and Lewi E (2025) Segmented dike intrusion linked to multi-level magma storage during and before the 2025 eruption at Erta Ale (East Africa).
Front. Earth Sci. 13:1719687.
doi: 10.3389/feart.2025.1719687

Segmented dike intrusion linked to multi-level magma storage during and before the 2025 eruption at Erta Ale (East Africa)

Alessandro La Rosa[1]*, Carolina Pagli[1], Derek Keir[2,3], Atalay Ayele[4], Hua Wang[5], Eleonora Rivalta[6,7] and Elias Lewi[4]

[1]Department of Earth Science, University of Pisa, Pisa, Italy, [2]School of Ocean and Earth Science, University of Southampton, Southampton, United Kingdom, [3]Department of Earth Science, University of Florence, Florence, Italy, [4]Institute of Geophysics, Space Science and Astronomy (IGSSA), Addis Ababa University, Addis Ababa, Ethiopia, [5]College of Natural Resources and Environment, South China Agricultural University, Guangzhou, China, [6]Physics of Earthquakes and Volcanoes, GFZ Helmholtz Centre for Geosciences, Potsdam, Germany, [7]Department of Physics and Astronomy, University of Bologna, Bologna, Italy

Introduction: Dike intrusions can assist continental rifting and plate divergence. However, our understanding of the magma dynamics during diking and the architecture of the magma storage that feeds dikes are still limited by temporally and spatially sparse dataset.
Method: In this study we used multiple evidence from InSAR, optical data, pixel offset tracking and seismicity to reconstruct the temporal evolution of the intrusion and the magma storage that fed the dike at the Erta Ale volcanic system (Afar Rift, East Africa), before and during the recent volcanic activity of July-August 2025.
Results: During 25 days, a dike propagated southward for 36 km, intruding a total of ~0.3 km^3 of mafic magma. InSAR modelling showed the dike intrusion was fed by multiple magma bodies, including a dike-shaped magmatic source and two shallow (~1 km) magmatic sills. InSAR time-series of the pre-diking period also revealed a deeper (~7 km) magmatic source that could have partially supplied the intrusion.
Discussion: The event, while much larger in volume, shows similarities to previous dike intrusions at Erta Ale, implying the presence of a long-lived multi-level magma storage system within the Erta Ale volcanic system.

KEYWORDS

dikes, InSAR, rift, East Africa, magma

1 Introduction

The intrusion of magma in the form of vertical dikes is the main mechanism for accommodating plate divergence in magma rich rift systems (e.g., Wright et al., 2012; Sigmundsson and Parks, 2024; Parks et al., 2025). Petrological and geophysical models show dikes commonly intrude perpendicular to the extension direction, fed from regions of magma ponding at various crustal levels within interconnected horizontal sills (Pagli et al., 2012; Wright et al., 2012; Cashman et al., 2017; La Rosa et al., 2024; Parks et al., 2025). While these models explain the overall mechanism of dike intrusion, our knowledge of the magma migration dynamics as well as the architecture and evolution of the

magmatic systems that feed dike intrusions is still limited by the temporal and spatial resolution of both geophysical and geological methods. In the last decades, geodetic methods such as Interferometric Synthetic Aperture Radar (InSAR) and Global Navigation Satellites System (GNSS) have been critical tools providing a better view of diking episodes on the exposed extensional plate boundaries of the East African Rift and Iceland (e.g., Wright et al., 2012; Pagli et al., 2012; Nobile et al., 2012; Sigmundsson et al., 2015; Sigmundsson and Parks, 2024; Xu et al., 2017; Moore et al., 2019). GNSS measurements can be made at high rates, even every few seconds, but only at discrete points making it hard to provide good spatial resolution. InSAR instead produces images of surface deformation over large areas of hundreds of km in scale, but the revisit time (~1 month) of past missions (e.g., the European ERS and Envisat) was often longer than the days-to-months intrusions time, providing only a static view of the temporally evolving dike dynamics. Recent SAR missions, as the European Sentinel-1 satellite, with a revisit time of 6–12 days can unveil the magma dynamics during diking. At present, only a few well documented examples exist in literature (e.g., Sigmundsson and Parks, 2024; Parks et al., 2025).

In July 2025 an eruption occurred in the Erta Ale volcanic system of the Afar Rift (Figure 1). The event was well observed by several satellite sensors that provided rare temporally dense coverage (Figure 1). Both optical sensors and local people observed the eruption starting on 15 July 2025 with caldera collapse and explosive eruption of ash and gasses (Figures 1B,H). The protracted emission of ash and gasses was accompanied by lava flows from the southern caldera rim on the 15 and 16 July, after which the flows progressively cooled (Figures 1C–H).

Here we use InSAR and seismicity to investigate the magma storage system beneath the Erta Ale segment and the dynamics of magma migration before and during the 2025 dike intrusion. To this aim we measured crustal deformation at Erta Ale from 2018 to 2025 spanning both the pre- and co-diking periods, using radar data from the European satellite Sentinel-1 (S1). We took advantage of the S1 frequent revisit time to analyze and model the temporal evolution of the diking process, the volumes of magma and the number of sources involved during 6–12 days time frames (Figure 2; Supplementary Figure S1). The 2025 event was preceded by another dike intrusion in 2017–2019 (Xu et al., 2017; Xu et al., 2020; Moore et al., 2019) and our InSAR time-series partially overlaps with this event allowing us to reconstruct the evolution of the plumbing system between the two intrusions. We found that the dike intrusion extended 36 km from the northern end of the Erta Ale lava lake and terminated at the Afrera linkage zone. The event lasted 25 days, during which the intrusion mobilized ~0.33 km^3 of magma and multiple magma bodies formed at various crustal levels. During the 6.5 years before the intrusion, from January 2018 to June 2025, inflation consistent with a sill expanding at 7.3 km depth is observed together with continuous dike opening below the lava lake.

2 Tectonic setting

The Erta Ale magmatic segment is a ~150 km-long, 40 km-wide ridge located in the northern sector of the Afar rift, a divergent plate boundary created by the separation of Arabia, Somalia, and Nubia plates (Figure 1A). The Erta Ale magmatic segment hosts six distinct volcanic centres: Dallol, Gada Ale, Alu-Dalafilla, Bora Ale, Hayli Gubbi and Erta Ale that gives the name to the entire magmatic segment (Barberi and Varet, 1970; Global Volcanism Program, 2023) (Figure 1). The magmatic segment is set within a sedimentary basin dominated by Pleistocene evaporites (Foubert et al., 2024; Rime et al., 2025). Both faulting and dike intrusions along the Erta Ale magmatic segment accommodate the divergence between the plates (e.g., Nobile et al., 2012; Pagli et al., 2012; Xu et al., 2017; Hurman et al., 2023; La Rosa et al., 2023), with associated eruptive fissures common along the rift (Acocella, 2006). Extensional rates in the Erta Ale magmatic segment increase southward, from ~6 mm/yr at latitude ~ N15° to ~14 mm/yr at the latitudes of Erta Ale (~N13.5°) (Figure 1; Viltres et al., 2020). The central sector of the magmatic segment is characterized by active volcanoes with shallow magma storage. Geochemistry and geodesy studies of Holocene-to-Recent eruptions at Alu-Dalafilla and Bora Ale showed the presence of magma bodies at depths between 1 and 4 km (Pagli et al., 2012; Watts et al., 2023). Protracted subsidence at Dallol has been explained by Kebede et al. (2025) with the deflation of a sill at a depth of 1.5 km. Similarly, the dike intrusion at Dallol in 2004 has been modelled to be fed by a source located at a depth of 2–3 km (Nobile et al., 2012). Further north however, normal faulting along fault-bounding grabens is observed in seismic reflection data to be important in extension (Hurman et al., 2023; Hurman et al., 2025), consistent with a tectonic seismic sequence of $M_w > 5$ having occurred north of Dallol in December 2022 (La Rosa et al., 2023). The southern end of the Erta Ale magmatic segment links to the Tat Ali one through an offset with oblique faulting and dike intrusions called the Afrera Plain (Figure 1; Illsley-Kemp et al., 2018; La Rosa et al., 2019; La Rosa et al., 2022).

Erta Ale has two NE-SW-elongated calderas, the Southern Caldera (SC) and the Northern Caldera (NC), that host a permanent and a transient lava lake, respectively (Figure 1). The volcanic system also includes the Ale Bagu strato-volcano and Hayli Gubbi shield volcano (Barberi and Varet, 1970; Xu et al., 2020). Seismic reflection/refraction data of the lithosphere beneath the Erta Ale magmatic segment imaged a 15 km-thick crust, the thinnest in the Afar rift (Makris and Ginzburg, 1987). The topography along Erta Ale varies from ~600 m a.s.l. at the calderas, to −80 m a.s.l. In the Afera Plain.

Historical records of the Erta Ale activity report volcanic eruptions, fluctuations of the lava lakes, lava flows and fumaroles since the 1940s (Barberi and Varet, 1970; Barberi et al., 1972; Barnie et al., 2016). High heat fluxes were measured during 2001–2002, in 2006 (Wright and Pilger, 2008) and a lake overflow was observed in 2010 (Field et al., 2012), while previous InSAR investigations over Erta Ale spanning 1993–1997 did not show clear evidence of either magmatic or tectonic deformation (Amelung et al., 2000). The first direct observations of a dike intrusion at Erta Ale are from 2004 when InSAR showed a sudden dike beneath the SC followed by progressive dike extension in 2008–2010 (Barnie et al., 2016). Then in 2017 another short (~3 km) dike intrusion occurred beneath the SC (Xu et al., 2017; Moore et al., 2019). The dike intrusion was preceded by replenishment of the NC dike from a deeper source during

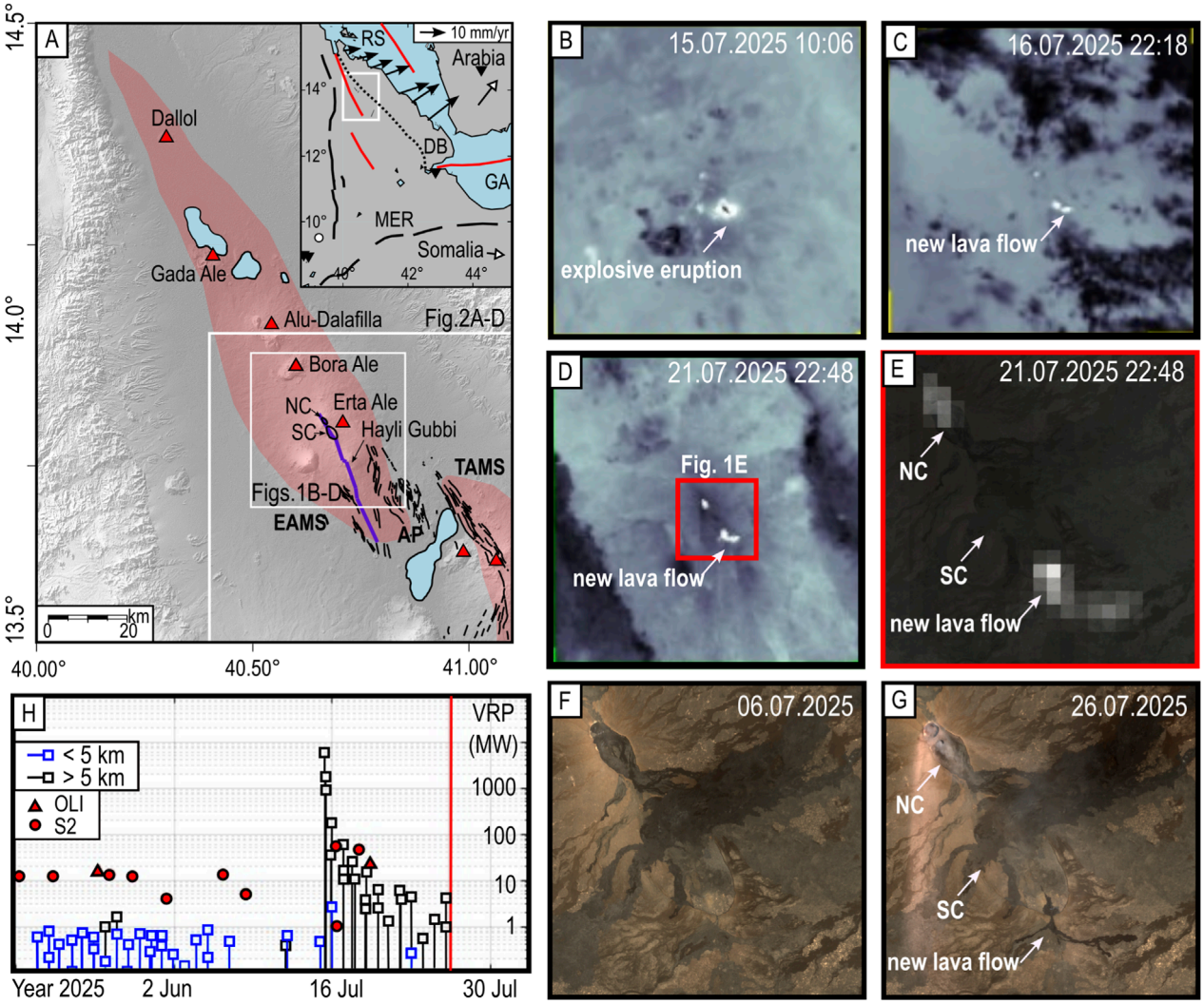

FIGURE 1
Tectonic setting and optical satellite acquisitions during the intrusion. **(A)** Shaded relief of Erta Ale magmatic segment. The shaded red polygons highlight the Erta Ale (EAMS) and Tat Ali (TAMS) magmatic segments. The red triangles are Holocene volcanoes from the Global Volcanism Program. The purple line is the 2025 dike path, while black lines are major faults. The inset shows the location of the study area (white box) and the main spreading centers (red lines). The black inverted triangles are the seismic stations used in the analysis, while the black and white arrows are GNSS velocities w.r.t. fixed Nubia (white dot) from Viltres et al. (2020). The black dashed line marks the Danakil Block (DB). **(B–E)** thermal anomalies detected by the Visible Infrared Imaging Radiometer Suite (VIIRS) 375 and reported by MIROVA (Coppola et al., 2016). The first thermal anomaly from the southern caldera was on **(B)** 15 July and the anomaly reached its final spatial extent by16 July **(B)**. The anomaly progressively reduced in amplitude through July, with the example in **(D)** for 21 July. **(F–G)** selection of Sentinel-2 cloud-free optical image in natural colors acquired before (06 July) and during (26 July) the dike intrusion. **(H)** Time series of thermal anomalies from MIROVA. The red symbols are the number of hot pixels within summit from Landsat-8 OLI (circles) and Sentinel-2 (S2, triangles) sensors. The stems are Volcanic Radiative Power (VRP) within 5 km from the summit (blue) and at more than 5 km from the summit (Coppola et al., 2016). NC, Northern Caldera, SC, Southern Caldera.

the previous 12 months (Xu et al., 2017; Moore et al., 2019). The dike event lasted until 2019 with the eruption of 10^7 m^3 of lavas (Moore et al., 2019) and widespread subsidence due to the depressurization of a trans-crustal plumbing system between depths of 4 and 11 km (Xu et al., 2020). Between 2019 and mid-2025, local witnesses report overflows of the permanent lava lake in 2023 and 2024 (Global Volcanism Program, 2023; Pin et al., 2024). Thermodynamic models from lavas samples suggest that eruptions and dike intrusion at Erta Ale are fed by a plumbing system extending to a ~15 km depth (Pin et al., 2024).

3 InSAR and seismicity analyses

We studied the co-eruptive period, 15 July – 9 August, analyzing 8 interferograms over the Erta Ale volcano processed from Sentinel-1 (S1) SAR data acquired in both ascending (orbit 014) and descending (orbit 079) geometry (Figure 2; Supplementary Figure S1). The shortest ascending interferograms span 6 days while for the descending geometry the shortest time span is 12 days. The interferograms were processed using the InSAR Scientific Computing Environment (ISCE2) software (Rosen et al., 2012)

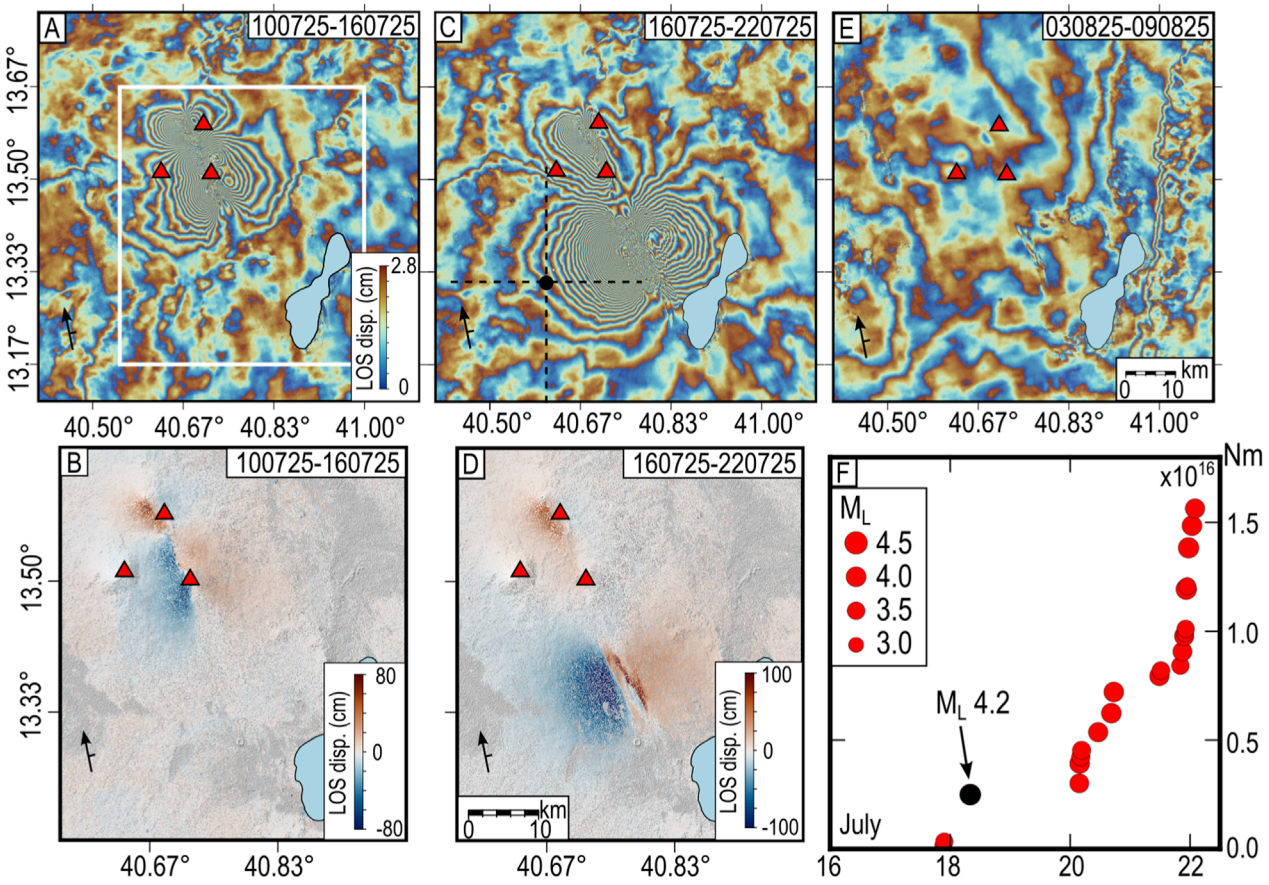

FIGURE 2
InSAR and seismicity during the 2025 dike intrusion at Erta Ale. **(A–E)** Wrapped S1 interferograms and range offsets for selected time-periods. A complete view of all time-periods is shown in Supplementary Figure S1. The time period spanned by the interferograms is in the upper right corner in ddmmyy format. Deformation in all the interferograms and range offsets is with respect to the satellite line-of-sight (LOS) and positive values mean a range increase (motion away from the satellite). The satellite orbit and the LOS are shown by the black arrow. The red triangles are Holocene volcanoes from the Global Volcanism Program as in Figure 1. The black dot in **(B)** is the M_L 4.2 earthquake of 18 July with related uncertainty (1σ) in the horizontal location (black dashed bars). **(F)** cumulative seismic moment release in Newton-meter (Nm) vs. time for the seismic sequence in July 2025.

and the Single Look Complex (SLC) SAR acquisitions were co-registered using a 30 m Shuttle Radar Topography Mission (SRTM) Digital Elevation Model (DEM, Farr et al., 2007). The interferometric phase was filtered using the Goldstein adaptive power spectral filter with strength of 0.5 (Goldstein and Werner, 1998) and then unwrapped using the ICU branch cut algorithm (Goldstein et al., 1988). The interferograms were finally geocoded using the 30 m SRTM DEM.

In addition to the interferograms, we performed Feature Point Offset Tracking (FPOT) and calculated range offsets between reference and secondary amplitude acquisitions (Figure 2; Supplementary Figures S2–S5; Peng et al., 2022). Standard OT methods are based on the identification of regular and evenly spaced tie points across the scene (e.g., Remie et al., 1999; Simons et al., 2002; Dzurisin and Lu, 2007). This approach has limitations when applied to fast-changing surfaces (e.g., croplands, forests and water bodies) as they cause mismatch between tie points and introduce noise. The novel FPOT method adopted here overcomes this limitation by identifying feature points that ensure high SNR offsets due to their distinct patterns (Peng et al., 2022). In general, range offsets are less accurate than interferograms but they provide supplementary measurements in areas of large deformation gradients where interferograms lose coherence. In our case, range offsets accuracy is ~1/20 of the SLC pixel spacing, corresponding to ~11 cm for S1 data. The final offsets maps were geocoded at a resolution of 90 m. Here we calculated range offsets from both ascending and descending acquisitions.

We also analysed the pre-eruptive period during the ~6.5 years preceding the intrusion (January 2018 - June 2025). We calculated time-series of cumulative Line-of-Sight (LOS) deformation and maps of average LOS velocity (Figure 3). To this aim, a total of 1180 S1A descending interferograms (orbit 079) with temporal baselines ranging 12–264 days were processed using the Parallel Small BAseline Subsets (P-SBAS) approach (Lanari et al., 2007) on the EarthConsole® cloud computing platform (De Luca, et al., 2024). For the processing, the topography-correlated atmospheric noise was removed by fitting the linear trend of phase delay with elevation (Elliott et al., 2008). The turbulent atmospheric component was then reduced by applying an Atmospheric Phase Screen (APS) filter (Ferretti et al., 2001; Lanari et al., 2007).

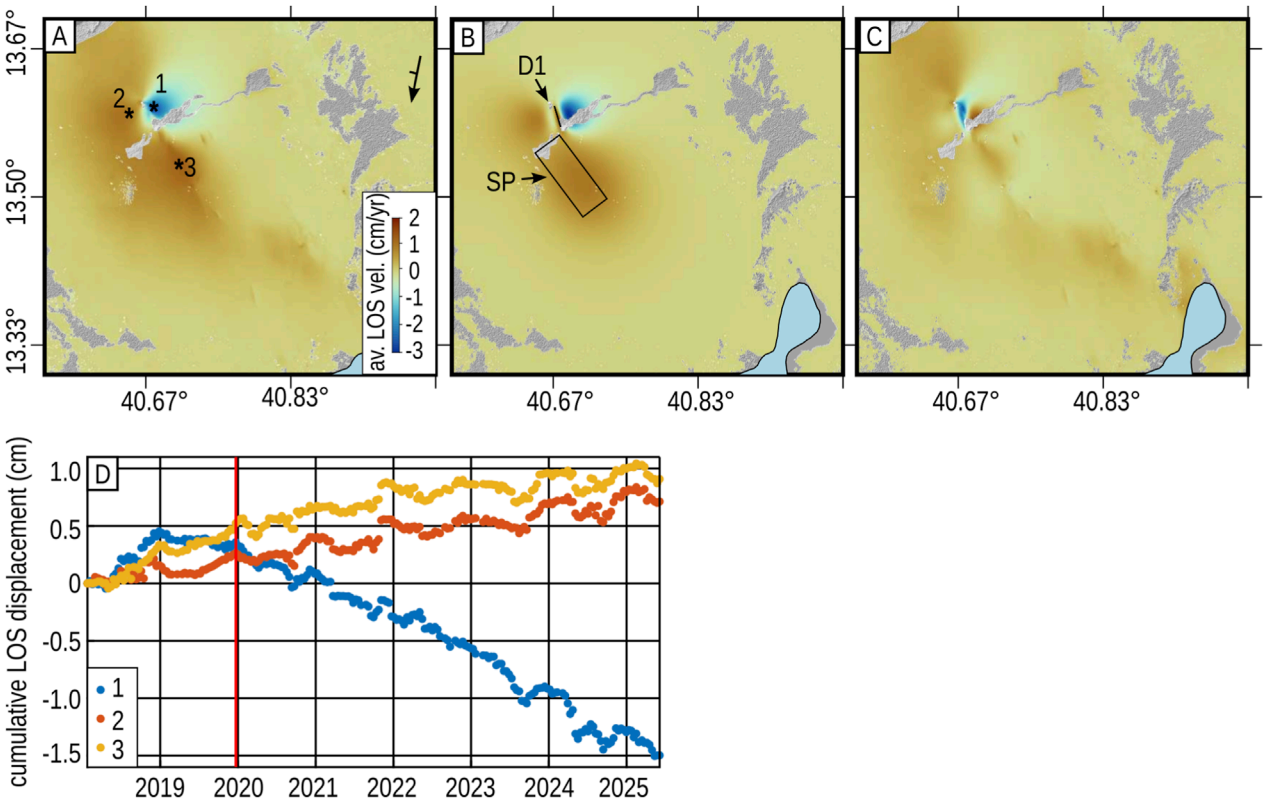

FIGURE 3
Observations and model of InSAR time-series for the pre-diking period. **(A)** Average LOS velocity map from descending orbit 079. The numbers refer to the three time-series in **(D)**. **(B)** Model with a uniform opening dike (D1, black line) and a contracting sill (SP, black rectangle). The best fit parameters of the sources are reported in Supplementary Table S1 **(C)** residual. The LOS velocity signals are unwrapped with positive changes indicating range increase. **(D)** time-series of cumulative LOS displacement from the three pixels in (a). The locations of the time-series are: 1) N13.5979°, E40.6746°; 2) N13.5958°, E40.6379°; 3) N13.5388°, E40.7038°.

For the seismic analysis, the continuous seismic data from the closest stations FURI (near Addis Ababa) and ATD (in Djibouti) were manually inspected from the start of 14 July to end of 9 August 2025. We identified twenty-two earthquakes with S-P time of ~67 s at FURI and ~43 s at ATD. These S-P times are consistent with earthquakes located in the Erta Ale region, at ~540 km and ~350 km distances from FURI and ATD, respectively. For these earthquake waveforms we simulated Wood-Anderson displacement seismograms, and then measured zero-peak amplitude. The amplitude and estimated distance from earthquake to stations were then used to compute local magnitude (M_L, Richter, 1935) (Figure 2F). We then computed seismic moment release using the empirical relation of Hanks and Kanamori (1979). For the largest earthquake of M_L 4.2 at 08:00 on 18 July, we could identify and pick P- and S-waves at 3 additional stations (AAE, ARAB and DAMY in Yemen), sufficient to derive an earthquake location. The earthquake was located 10 km south of Erta Ale with location error 19.3 km in longitude and 25.5 km in latitude, consistent with the earthquake to be associated with the dike (Figure 2C). Analyzing the frequency content of the earthquake signals can shed light on their nature (tectonic vs. magmatic). In particular, low frequency events can be associated with migration of magma in the crust, while high-frequency earthquakes are more typical of brittle failure (e.g., Hensch et al., 2019; Firetto Carlino et al., 2025; Isken et al., 2025). Here we analyzed the frequency content of the largest earthquake to infer the magmatic or tectonic origin of the event (Supplementary Figure S7).

3.1 Pre-diking period: January 2018-June 2025

Average LOS velocities from descending orbit show two main deformation patterns at Erta Ale (Figure 3). At the NC, the pattern consists of a main lobe with range decrease of ~2.6 cm/yr on the northeastern side and a zone of range increase of ~1.0 cm/yr on the southwestern side. This signal is consistent with extension by a ~NS-striking dike. Just south of this signal, a broad concentric range increase pattern with rates of ~1.2 cm/yr is observed between the SC and Hayli Gubbi, suggesting the presence of a deflating source (Figure 3A). The time-series of pixels above the dike show the deformation started in January 2020 and continued until the eruption at approximately linear rates (Figure 3D). The temporal pattern of the sill deflation is different from the dike (Figure 3D) and it started at the beginning of our observation period in January 2018.

3.2 Co-diking period: July-August 2025

The first evidence of diking at Erta Ale is shown by an ascending interferogram spanning 10–16 July where two adjacent deformation patterns are observed along a ~20 km long sector of the Erta Ale calderas (Figures 2A,B). The largest signal at the SC has two lobes with up to ~53 cm of range increase in the satellite Line-of-Sight (LOS) on the southwestern side of the caldera and ~33 cm of range increase on the northeastern side (Figure 2A), consistent with a ~NS intruding dike along the central axis of the Erta Ale volcanic centre. At the NC, a similar two-lobe pattern is observed but with opposite polarities on both flanks of the caldera, up to ~30 cm of range increase on the southwestern side of the caldera, and up to ~15 cm of range decrease on the northeastern side (Figure 2A). This pattern is consistent with a ~NS contracting dike. A consistent deformation pattern is also observed in a descending interferogram spanning 9–21 July (Supplementary Figure S1H). An ascending interferogram spanning 16–22 July shows deformation from the intruding dike which propagated ~20 km southeast-ward along the Erta Ale magmatic segment axis reaching the Afrera Plain (Figure 2B). The magnitude of the deformation also increased with up to ~100 cm of range decrease observed on the southwest and a ~39 cm range increase on the northeast. The signal from the contracting dike at the Erta Ale caldera also lengthened southeast-ward.

Since 22 July just small deformation from the contracting dike is observed at the Erta Ale caldera and deformation starts decaying in the dike intruding area, in the Afrera Plain, until stopping on 9 August 20205 (Supplementary Figure S1; Figure 2E). Furthermore, both ascending and descending 12-days interferograms show two circular patterns of range decrease with values up to 6.5 cm at the SC and at Hayli Gubbi, consistent with vertical motions likely caused by inflating shallow sources (Supplementary Figure S1F,H). However, we do not have clues about their inception time.

Strong changes in the reflective properties of the ground (e.g., building collapses, lava flows, surface fracturing and large deformation) during the time period between two SAR acquisitions introduce dissimilarity in the pixel's phase, and can be measured by the phase coherence (Hanssen, 2001; Simons et al., 2002; Dzurisin and Lu, 2007; Dietterich et al., 2012). To better understand the surface deformation, we analyzed the InSAR phase coherence images to identify changes caused by the newly erupted lava flows and the areas of fracturing above the dike. We identify different regions of low coherence between 10 and 16 July. Along the axial sector of Erta Ale, the low coherence is arranged in a segmented linear pattern, compatible with the surface fracturing caused by the intrusion. Two circular patterns of low coherence are also observed at the two calderas (Figures 4A,B) and are consistent with the caldera collapses reported at the NC and SC. Both patterns are surrounded by larger concentric areas, ~2 km^2 and ~8 km^2, of low coherence that progressively decay at the margins, likely associated with the deposition of erupted products during the initial explosive activity (e.g., Naranjo et al., 2022). Finally, a distinct area of low coherence, ~1 km^2, corresponds to the lava flowing eastward, likely fed by a vent located within the SC (Figure 4B).

From 16 to 22 July, a concentric area of low coherence is observed NW of the NC, consistent with further deposition of erupted products. Also, low coherence is observed on the lava flow and along the NE margin of the SC compatible with faulting and further caldera collapse. A new area of low-coherence is also observed further south likely caused by axial fracturing above a dike (Figure 4C). From 22 July onwards, the area around Erta Ale does not show further changes in the coherence while the southern sector shows coherence progressively increasing as rate of deformation decays. The coherence in the south is consistent with the observed seismicity. Earthquakes were only observed from near the end of 17 July to early on 22 July, with notable peaks in seismic activity at the start of 20 July and the end of 21 July (Figure 2F). Estimates of the local earthquake magnitudes show that they are between M_L 3.3–4.2. The total seismic moment release is relatively low at 1.6×10^{16} Nm. The location and frequency content of the M_L 4.2 earthquake and timing of all seismicity suggest faulting was only associated with intrusion of the southernmost segment of the dike, and that these were associated with the initial propagation of the dike.

4 InSAR modelling

We modeled both the pre-diking and co-diking interferograms, range offsets, and maps of average LOS velocity. For the modelling, we used a non-linear Monte Carlo simulated annealing inversion followed by a derivative based procedure weighted for the variance of the signal noise (Cervelli et al., 2001). Before the inversion, the interferograms, the LOS velocity map and the range offsets were sub-sampled using a quad-tree partitioning algorithm based on the data variance (Jonsson et al., 2002). We explained the deformation by using different combinations of Okada tensile dislocations (Okada, 1985) buried in an elastic half-space with shear modulus of 30 GPa and a Poisson's ratio of 0.25.

For the co-diking phase, we initially inferred the number and the geometry of the sources by joint inversion of 12-day ascending and descending interferograms and range offsets, assuming uniform opening/contraction of the Okada tensile dislocations (Supplementary Figure S2). For the ascending orbit, we stacked two consecutive 6-day interferograms to obtain 12-day interferograms that span nearly the same period as the descending interferograms, with a difference of only 1 day. Stacking also reduces noise. We used the coherence maps to set the number of sources and the search bounds of the inversion. We then modelled the spatially variable dike opening/contraction by linear least-squares inversion of ascending interferograms and range offsets (Supplementary Figure S3), fixing the source geometry based on the uniform models and discretizing the Okada dislocations into patches of 0.5 km × 0.5 km (Figures 5, 6). For the early co-diking period from 10 to 22 July when dike propagation was fast, we modelled the shortest 6-day interferograms, while we used variable temporal resolutions between 6 and 12 days during the later phases.

For the pre-diking phase, we inverted the map of average LOS velocity from descending orbit assuming uniform opening/contraction of two Okada dislocations to fit the two main deformation patterns (Figure 3). We used a vertical (dip angle equal to 90°) opening source to fit the pattern at NC and a contracting horizontal (dip angle equal to 0°) source to fit the signal between SC and Hayli Gubbi. We then inverted for the best-fit location, strike, shape and opening parameters by searching within relatively large bounds.

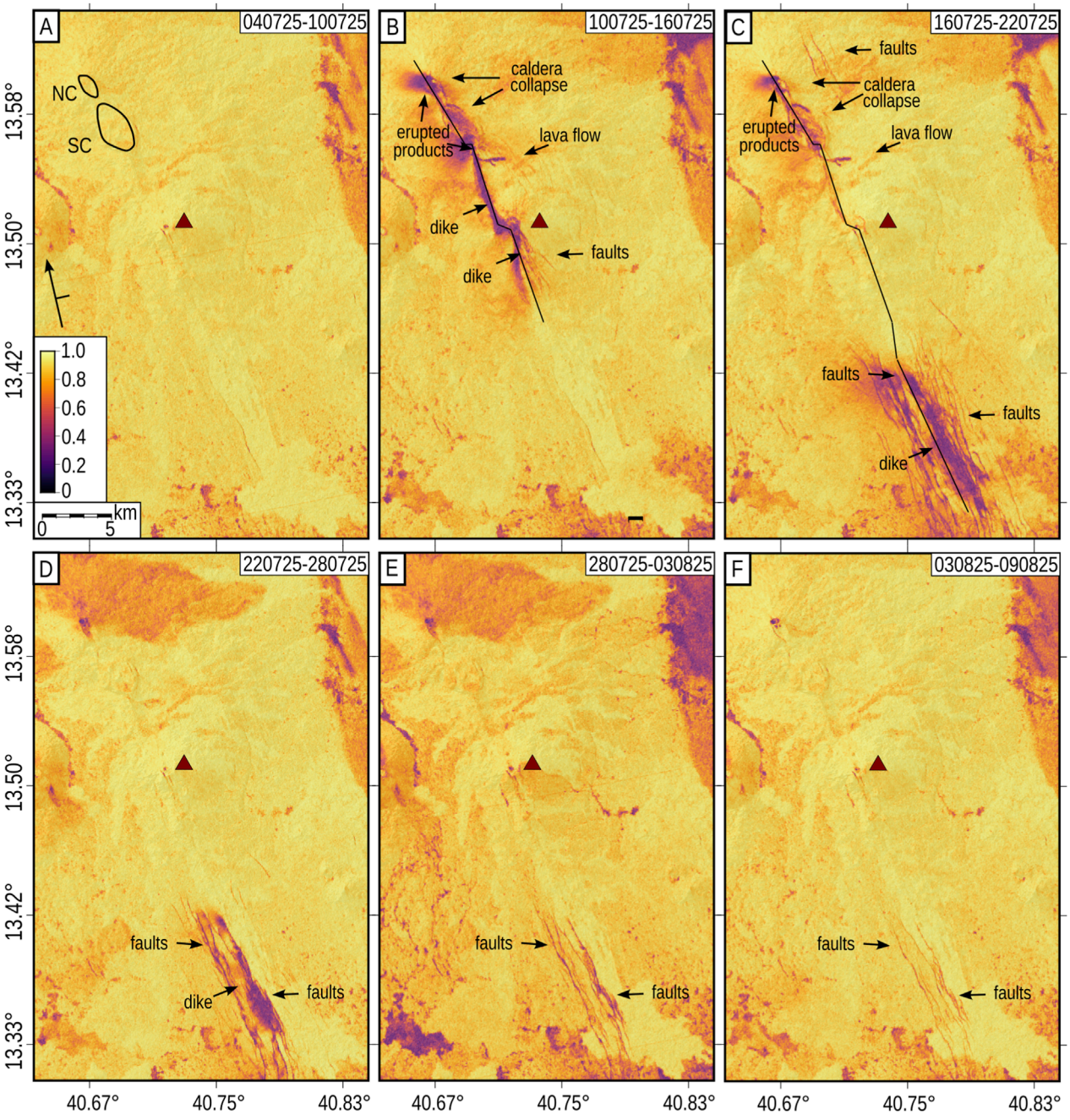

FIGURE 4
Ascending maps of phase coherence during 6 days time frames **(A–F)**. The time periods are reported in the top-right corner of each panel in ddmmyy format. Darker tones mark the low coherence induced by changes between the reference and secondary SAR acquisition, while high coherence values indicate no changes. Panel **(A)** shows a coherence map before the inception of the intrusion, as a reference. In each panel, we indicate the interpreted processes causing changes in the coherence. The two black polygons in **(A)** mark the Northern Caldera (NC) and Southern Caldera (SC). The black solid lines in **(B,C)** mark the projection of the distributed model at the surface. The red triangle is Hayli Gubbi.

4.1 Pre-diking modelling: January 2018-June 2025

During the pre-diking period, the deformation at Erta Ale is best explained by a ~2.7 km-long, 1 km-wide dike striking N163°E (Figures 3A–C; Supplementary Table S1). The dike is located beneath the NC, and the upper edge of the dike is at ~0.8 km depth. The dike opening was time-progressive and occurred at a constant rate of ~30 cm/yr, corresponding to a total opening of 1.62 m and volume of intruded magma of ~0.005 km^3 from January 2020 to June 2025 (Figure 3D). Further south, the subsidence pattern between the SC and Hayli Gubbi is fitted by a 9.9 km-long, 3.7-km-wide deflating sill located at a depth of ~7.4 km (Figures 3A–C; Supplementary Table S1). The sill deflated with a rate of ~5.5 cm/yr

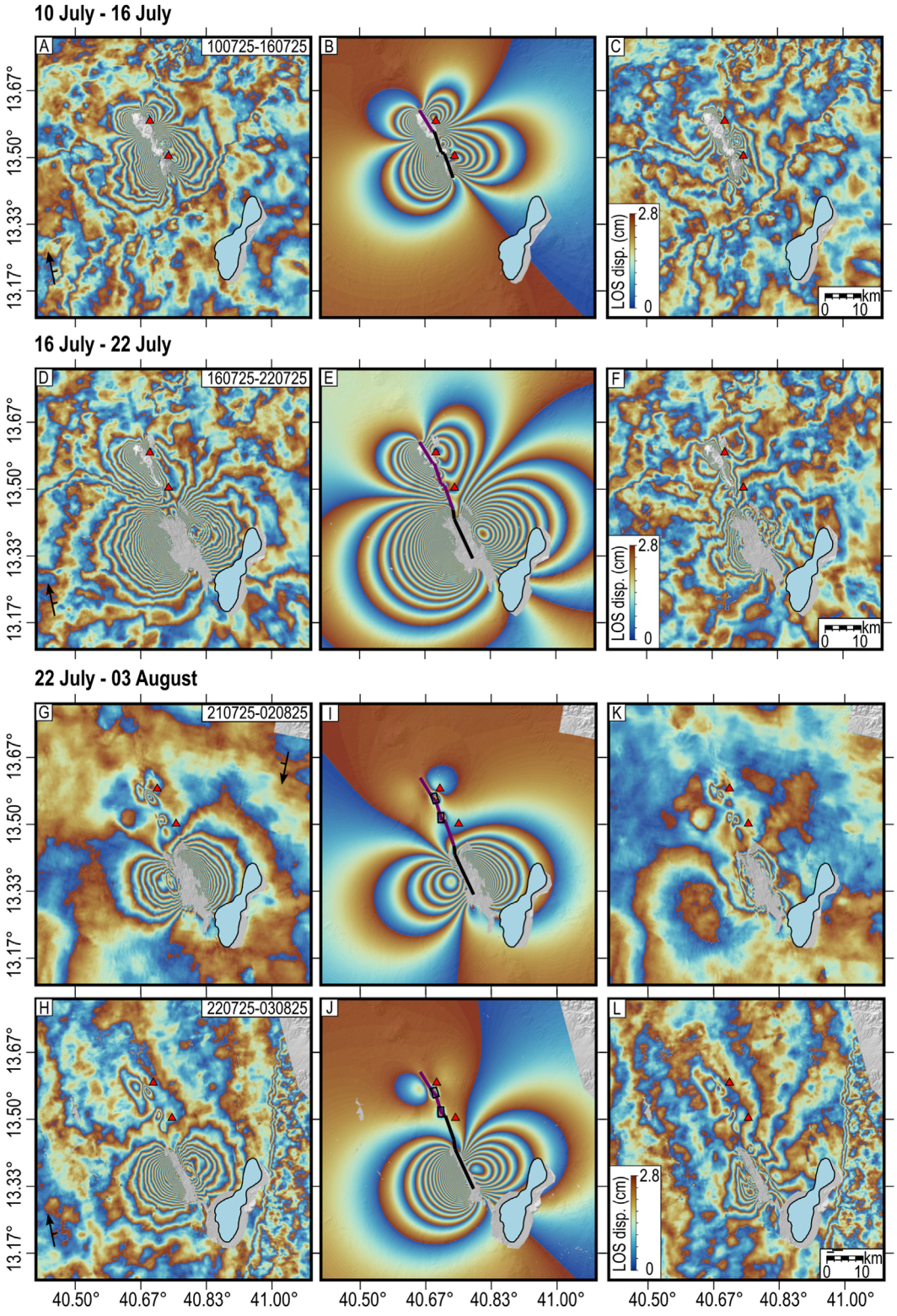

FIGURE 5
Distributed modelling results. **(A–C)** InSAR ascending observation, model and residual for the early dike intrusion (10–16 July). **(D–F)** InSAR ascending observation, model and residual for the mid dike intrusion (16–22 July). A complete view of the results including the range offsets is shown in Supplementary Figures S3–S5. **(G–L)** InSAR observation, model and residual for the late dike intrusion (22 July-03 August) from both descending and ascending geometries. The LOS displacement signals are wrapped with positive changes indicating range increase. The red triangles mark the Erta Ale and Hayli Gubbi volcanoes. The black arrows indicate the satellite viewing geometry. The purple and black lines mark the closing opening and closing sectors of the dike, respectively, while the black rectangles are the sill projection at the surface.

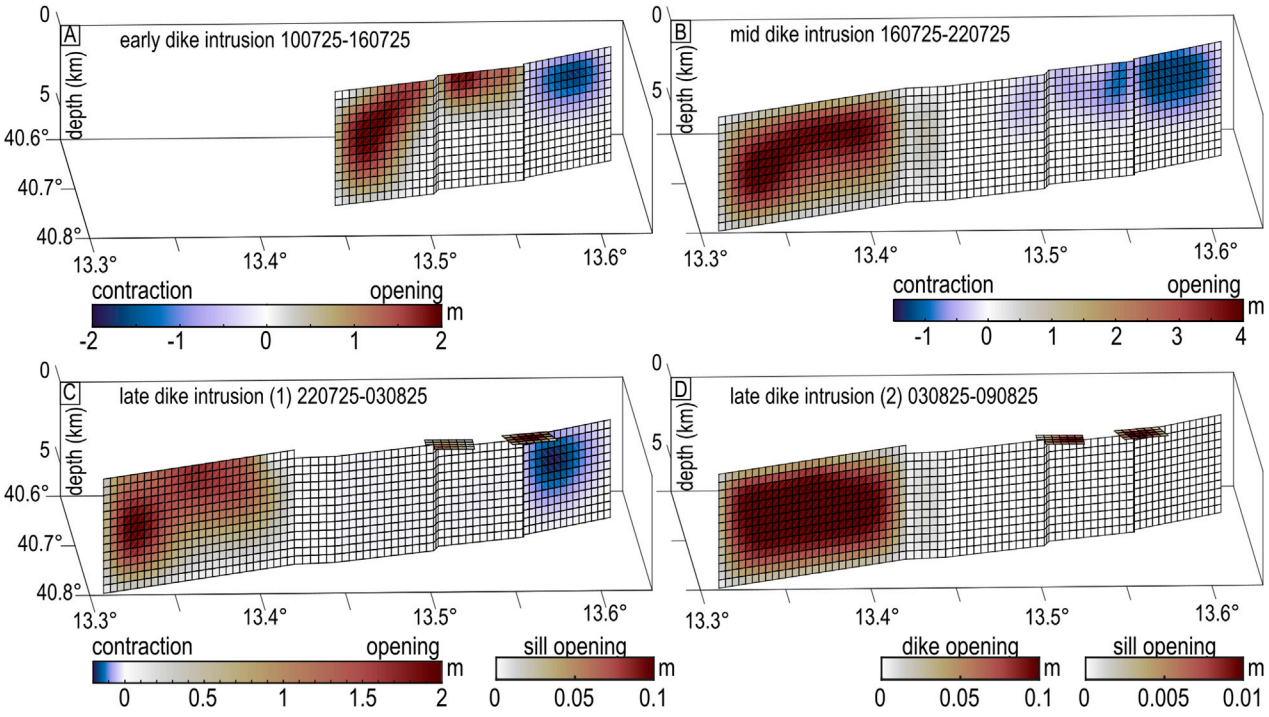

FIGURE 6
Models of distributed dike opening/contraction and sill opening, during the main phases of the dike intrusion. **(A)** dike opening/contraction during 10–16 July. **(B)** dike opening/contraction during 16–22 July. **(C)** dike opening/contraction and sill opening during 22 July-03 August. **(D)** dike and sill contraction during 03–09 August. The top depth of the contracting section of the dike has been set to 1 km to include sills in the model and avoid cross-cutting sources. Dates are reported in ddmmyy format. The colorbars have different bounds across the dike phases to better highlight the opening/contraction patterns.

corresponding to a total volume of drained magma of ~0.3 km^3 from 2018 to June 2025 (Figure 3D; Supplementary Table S2).

4.2 Co-diking modelling: July-August 2025

The deformation is best explained by a model consisting of up to four en-echelon dike segments striking in an average ~ N157°E direction (Supplementary Figures S2, S3; Supplementary Table S1). The segments extend from the surface (~0–0.5 km) to a depth of ~6 km and some experience extension while others contract (Supplementary Table S1). In the uniform modelling the dike segments are separate with only small strikes differences, between N149°E and N162°E (Supplementary Figure S2; Supplementary Table S1) while for the distributed modelling we connected the dike segments and also extended them down to a depth of 7 km (Figures 5,6, ; Supplementary Figures S3–S4).

Our preferred model for the initial diking period, between 10 and 16 July, consists of three dike segments. A ~7-km long dike segment beneath the NC contracts up to ~1.7 m, while two dike segments (~11 km-long in total) open further southwest beneath the SC and Hayli Gubbi (Figures 5A, 6a; Supplementary Figure S4). The two dike segments have a distributed opening of up to ~2 m, corresponding to a volume of intruded magma of ~0.21 km^3, while the total volume of drained magma from the contracting dike is an order of magnitude lower (~0.021 km^3) (Supplementary Table S2). The model has a root-mean-square (rms) residual of ~4 cm for the InSAR and ~10 cm for the range offsets.

During 16–22 July, the best fit-model includes an additional ~15 km-long dike segment striking N155°E and opening further southwest up to 4 m (Figure 6b). The dike opening corresponds to the intrusion of 0.24 km^3 of magma. At the same time, the dike segments at Erta Ale and Hayli Gubbi switched to contraction up to ~1.5 m, with a total volume of drained magma equal to ~0.038 km^3 (Supplementary Table S2). The model leaves a root-mean-square (rms) residual of ~4 cm for the InSAR data and ~18 cm for the range offsets. The residuals are mainly related to shallow faulting at the southern dike that we did not consider in our models, while the large-scale signals caused by the intrusion remain well-fitted (Figure 5C; Supplementary Figure S5).

Between 22 July and 9 August, the best fit-model shows additional opening of the southern dike up to ~1.8 m within the first 12 days (22 July – 3 August) and no further propagation (Figures 6c,d). The opening corresponds to a volume of intruded magma of 0.09 km^3, while negligible dike contraction of 0–20 cm and the drainage of ~0.0034 km^3 of magma is modelled further north. The two circular range decrease signals observed at the SC and Hayli Gubbi are fitted best by two inflating sills oriented N165°E and N181°E and located at depth of 0.95 km and 0.85 km, respectively (Supplementary Table S1). The model of distributed deformation of 3 km-long x 2 km-wide sills show opening up to 40 cm at the SC and 10 cm at Hayli Gubbi, corresponding to

total volume changes of 0.0004 km^3 and 0.0002 km^3, respectively (Supplementary Table S2). The model leaves a root-mean-square (rms) residual of ~3 cm for both ascending and descending interferogram. As above, the residuals are mainly observed at the southern dike segment and are related to shallow faulting that we did not consider in our models, while the large scale signals caused by the intrusion as also the shallow inflating sills are well-fitted (Figures 4K,L). The same sources fit the deformation patterns observed until 9 August (Supplementary Figure S6) with a small opening of the southern dike (~10 cm) and the two sills (~1–4 cm).

5 Discussion

We used evidence from InSAR, pixel offsets tracking, optical data and seismicity to investigate the dynamics of magma motion at Erta Ale during the eruptive and diking episode of July-August 2025 and the 6.5 years before it. We show that between January 2018 and June 2025, a large sill contracted at a depth of 7.3 km beneath the SC and Hayli Gubbi, while a dike beneath the NC has inflated at rates of ~0.0008 km^3/yr, corresponding to a total volume of ~0.005 km^3. A sill at a similar depth (4–11 km) was inferred during 2018 - June 2019, likely feeding the protracted lava flows in 2019 (Moore et al., 2019; Xu et al., 2020). Conversely, no evidence of dike opening was reported during the later phases (Moore et al., 2019; Xu et al., 2020). Our InSAR time-series partially overlaps with this late phase showing the opening of the NC dike resuming in 2020. The similarities between our model and those presented by Xu et al. (2020) could indicate that the deeper sources of 2017–2019 and 2025 are either the same, remaining active during 2019–2025, or located nearby. We envisage that the sill has deflated as it partly fed magma into a dike above it since January 2020. Before the 2025 intrusion, local witnesses reported two lava lake overflows in 2023 and 2024. Those two events lack detailed descriptions in literature but the two episodes could be related to the dike pressurization and hydraulic connection with the lava lake, as already inferred for past lake overflows (Moore et al., 2019).

The dike intrusion started sometime between 10 and 16 July accompanied by caldera collapse, explosive eruption and a lava flow from the SC rim on 15 July. The inversion of co-diking deformation shows that the formerly opening NC dike switched to contraction during the early intrusion, draining magma toward a ~14 km segmented dike beneath the SC and Hayli Gubbi. Our models indicate that ~0.21 km^3 intruded the southern segments against 0.021 km^3 of magma drained from the NC dike. The opening segments reached the surface causing the eruption of a lava flow from the SC. Similar dynamics and magmatic sources characterized the intrusion of 2017 (Xu et al., 2017; Moore et al., 2019) but that event remained confined within the two calderas. Furthermore, the existence of a contracting dike at the NC was already inferred by Barnie et al. (2016) based on the reconstruction of past eruptions. It is thus possible that the northern dike is the same long-lived feature that was activated in the past. Magma accumulation zones shaped as vertical dikes are unusual but not exclusive to Erta Ale. A prominent basaltic example is Mauna Loa, where magma accumulation in a dike-shaped reservoir happened during 2002–2021 and fed a fissure eruption in November 2022 (Amelung et al., 2007; Varugu and Amelung, 2021; Ellis et al., 2025). Petrological evidence suggests that Mauna Loa's shallow magma storage geometry may have been stable for the last 10 k years (Wieser et al., 2025). An example of explosive, silicic eruption fed by the contraction of a dike-shaped source is the 2015 eruption at Calbuco volcano in Chile (Nikkhoo et al., 2017). At Mauna Loa, tensile stresses promoting magma accumulation in a dike-shaped reservoir is provided by flank dynamics (Amelung et al., 2007), while at Erta Ale regional extension and an elongated edifice shape may provide the key stress contributions controlling the magma storage and pathway architecture and eruptive patterns (Rivalta et al., 2019).

From 16 to 22 July, the intrusion propagated ~15 km toward the Afrera Plain, becoming the largest dike intrusion ever observed directly at the Erta Ale magmatic segment. The dike stopped ~9 km north of the Afrera town and opened up to ~4 m (Figure 6B) with the volume of the intrusion being ~0.33 km^3 of magma (Supplementary Table S2). At its full length, the dike opened in an average N67° ± 6°E direction, parallel to the regional extension direction (Viltres et al., 2020). The dike propagation was accompanied by shallow normal faulting above it, as shown by narrow bands of range increase in both ascending and descending range offsets, and the observed seismicity during 17–22 July (Supplementary Figure S3C,D,S5). The waveform and spectrogram of the M_L 4.2 earthquake (Supplementary Figure S7) shows that the that the spectrum of the earthquake was rich in low frequencies but had very little energy above 1 Hz. Earthquakes with similar frequency contents are common of magma-induced faulting (Pallister et al., 2010). Estimations of lateral dike propagation velocity are possible for the time period 16–22 July, whose time frame and opening are well constrained. Assuming the opening of the southern dike was uniform during the 6 days satellite revisit time, its 15 km length gives an average lateral propagation velocity of ~1.74 m/s. This velocity is higher than the basaltic intrusions in Ethiopia, the Dabbahu-Manda-Harraro in 2005–2010 (0.14–0.83 m/s, Grandin et al., 2011) and Fentale-Dofen in September 2024 (0.004 m/s, Keir et al., 2025). Instead in Iceland, basaltic magma propagated at velocities up to1.3 m/s during the Bardarbunga dike intrusion of 2014–2015 (e.g., Ágústsdóttir et al., 2016; Eibl et al., 2017), similar to the Erta Ale dike. Ultrafast dike propagation was also observed during the Novembre 2023 intrusion in Grindavik (Iceland), where record velocity reached 2.46 m/s (Sigmundsson and Parks, 2024). Magma can flow at high rates if it tensile stresses are high, if caldera collapses occur above the feeding source, or if the magma viscosity is low (Sigmundsson and Parks, 2024). The above comparison with previous basaltic intrusion suggests that the 2025 dike has mobilized low viscosity basaltic magmas. Furthermore, the 2025 diking occurred in a sector of the Erta Ale ridge that did not experience any recent intrusion and likely accumulated high tensile stresses from the long-term tectonic extension. High tectonic stress build-up could thus be another factor explaining the fast dike intrusion of Erta Ale as also observed in Iceland (Sigmundsson and Parks, 2024). While propagating southward, the dike contracted at its northern end and the contraction also migrated southward, such that dike segments that initially opened then closed. This is also shown by the progressively increasing InSAR coherence due to decaying dike opening at the northern segments. Contraction of the tail of a propagating dike has been theorized, especially for low-viscosity magmas, and inferred based on seismicity patterns and numerical

modelling (e.g., Maccaferri et al., 2016) but it has never been directly observed. It is possible that this process occurred in the past but that the deformation was not measured. This may be important to consider in future inversions.

Later during the intrusion, from 22 July - 9 August, additional 0.09 km^3 of magma were intruded in the southern dike segments while ~0.0034 km^3 of magma were drained from the northern segments. Between the southern and northern dike segments, two shallow sills at a depth of ~1 km beneath the SC and Hayli Gubbi inflated, indicating that storage below Erta Ale is a complex system of dikes and sills. The presence of a sill at the same depth at the SC have been inferred also during the late stages of the 2017 dike intrusion (Xu et al., 2017) and by petrological analysis of the 2010 eruption (Field et al., 2012). Furthermore, during the later stages of the intrusion we see disconnected dike segments deforming, the northern segments contracted while the southern segments opened but no dike deformation was observed midway between the two sectors. We envisage that magma flow occurred in the mid-section but without any further opening (Figures 5C,D). Sill inflation is in fact observed in the mid-segments indicating that magma was still flowing in the sector.

The total volume of magma intruded during the 2025 dike intrusion is ~0.33 km^3 (Supplementary Table S2) while the volume of magma intruded into the NC dike during January 2020 - June 2025 was two orders of magnitude lower. Lower volume discrepancies up to factors of 4-5 are often observed between intruding dike and contracting sources (e.g., Wright et al., 2006; Rivalta and Segall, 2008). Physical models can easily explain these differences invoking magma compressibility or stiffness of the host-rock, but larger discrepancies need alternative explanations, such as the presence of additional magma sources. While the co-diking deformation is well explained by the dike itself and does not call for the presence of a deeper source, the magma drained from the NC dike is not enough to supply the large dike intrusion further south. It is possible that the deeper sill modelled during 2018–2025 remained active during the whole intrusion period but its deformation signal was either too weak or hidden by the shallower sources to be resolved. The InSAR data and models show that the vast majority of extension was accommodated by the dike, with minor faulting likely restricted to the southern tip of the dike, also in agreement with the relatively low seismicity, only one earthquake magnitude 4.2. This is consistent with that interpreted over decadal time-scales, with the modeled ratio of 0.02 between seismic and aseismic extension in Northern Afar over the last ~70 years (Hurman et al., 2025).

The similarities in the dynamics of the intrusion in the 2025, 2017 and earlier events (Xu et al., 2017; 2020; Moore et al., 2019; Barnie et al., 2016) indicates that diking episodes at EA likely result from the presence of a multi-level storage magmatic systems of hydraulically connected sills and dikes, consistent with the geochemistry of volcanic rocks at Erta Ale (Pin et al., 2024). This multi-level storage system supplies magma to intrusions and eruptions at EA and it is stable and likely long-lived.

6 Conclusion

In this study, we combined a temporally dense dataset from various satellite techniques with seismicity to investigate the magma dynamics and the evolution of the feeding magmatic system during the July-August 2025 dike intrusion at the Erta Ale magmatic segment. Starting from 15 July, the dike fed an explosive eruption and a lava flow while propagating southwards along the axis of the magmatic segment. The intrusion of 0.33 km^3 of basaltic magma was fed by a contracting dike below the NC and probably by a deeper sill at a depth of ~7 km. The event lasted 25 days during which the dike accommodated more than 4 m of plate extension and propagated at a minimum velocity 1.74 m/s. While advancing, the opening of new dike segments was accompanied by the closure of the back parts of the dike. During the final stages of the intrusion magma migrated toward shallower sills at a depth of ~1 km while only the southern dike sector kept opening. The event was the largest ever observed directly at the Erta Ale magmatic segment and revealed the presence of a hydraulically connected and long-lived multi-level magma storage system that feeds dike intrusions beneath the EA volcanic system.

Data availability statement

The original contributions presented in the study are included in the article/Supplementary Material, further inquiries can be directed to the corresponding author.

Author contributions

AL: Investigation, Conceptualization, Writing – review and editing, Formal Analysis, Writing – original draft, Data curation, Visualization. CP: Writing – original draft, Formal Analysis, Writing – review and editing, Investigation, Conceptualization. DK: Investigation, Writing – review and editing, Visualization, Formal Analysis, Writing – original draft. AA: Visualization, Formal Analysis, Writing – review and editing, Writing – original draft. HW: Writing – original draft, Software, Writing – review and editing. ER: Writing – original draft, Writing – review and editing. EL: Writing – review and editing, Writing – original draft.

Funding

The authors declare that financial support was received for the research and/or publication of this article. ALR and CP are supported by the Space It Up project funded by the Italian Space Agency (ASI) and the Ministry of University and Research (MUR) under contract n. 2024-5-E.0 CUP n. I53D24000060005. The work is affiliated to the ADD-ON Project https://www.afardalloldrilling.com/). HW is supported by the National Natural Science Foundation of China (42274001) and the Associates Program by ICTP and the Simons Foundation (284558FY19).

Conflict of interest

The authors declare that the research was conducted in the absence of any commercial or financial relationships that could be construed as a potential conflict of interest.

The author(s) declared that they were an editorial board member of Frontiers, at the time of submission. This had no impact on the peer review process and the final decision.

The handling editor JM declared a past co-authorship with the author DK.

Generative AI statement

The authors declare that no Generative AI was used in the creation of this manuscript.

Any alternative text (alt text) provided alongside figures in this article has been generated by Frontiers with the support of artificial intelligence and reasonable efforts have been made to ensure accuracy, including review by the authors wherever possible. If you identify any issues, please contact us.

Publisher's note

Supplementary material

The Supplementary Material for this article can be found online at: https://www.frontiersin.org/articles/10.3389/feart.2025.1719687/full#supplementary-material

References

Acocella, V. (2006). Regional and local tectonics at erta ale caldera, Afar (Ethiopia). *J. Struct. Geol.* 28, 1808–1820. doi:10.1016/j.jsg.2006.06.014

Ágústsdóttir, T., Woods, J., Greenfield, T., Green, R. G., White, R. S., Winder, T., et al. (2016). Strike-slip faulting during the 2014 bárðarbunga-holuhraun dike intrusion, central Iceland. *Geophys. Res. Lett.* 43, 1495–1503. doi:10.1002/2015GL067423

Amelung, F., Oppenheimer, C., Segall, P., and Zebker, H. (2000). Ground deformation near gada 'ale volcano, Afar, observed by radar interferometry. *Geophys. Res. Lett.* 27 (19), 3093–3096. doi:10.1029/2000GL008497

Amelung, F., Yun, S., Walter, T. R., Segall, P., and Kim, S. (2007). Stress control of deep rift intrusion at Mauna Loa volcano, Hawaii. *Science* 316 (5827), 1026–1030. doi:10.1126/science.1140035

Barberi, F., and Varet, J. (1970). The erta ale volcanic range (danakil depression, Northern Afar, Ethiopia). *Bull. Volcanol.* 34(4), 848–917. doi:10.1007/BF02596805

Barberi, F., Borsi, S., Ferrara, G., Marinelli, G., Santacroce, R., Tazieff, H., et al. (1972). Evolution of the danakil depression (Afar, Ethiopia) in light of radiometric age determinations. *J. Geol.* 80 (6), 720–729. doi:10.1086/627797

Barnie, T., Oppenheimer, C., and Pagli, C. (2016). Does the lava Lake of erta 'ale volcano respond to regional magmatic and tectonic events? An investigation using Earth observation data. London, UK: Geological Society Publications 420 (1), 181–208. doi:10.1144/SP420.15

Cashman, K. V., Sparks, R. S. J., and Blundy, J. D. (2017). Vertically extensive and unstable magmatic systems: a unified view of igneous processes. *Science* 355, eaag3055. doi:10.1126/science.aag3055

Cervelli, P., Murray, M. H., Segall, P., Aoki, Y., and Kato, T. (2001). Estimating source parameters from deformation data, with an application to the March 1997 earthquake swarm off the izu peninsula, Japan. *J. Geophys. Res. Solid Earth* 106 (B6), 11217–11237. doi:10.1029/2000JB900399

Coppola, D., Laiolo, M., Cigolini, C., Delle Donne, D., and Ripepe, M. (2016). Enhanced volcanic hot-spot detection using MODIS IR data: results from the MIROVA system. *Geol Soc* 426, 181–205. doi:10.1144/SP426.5

De Luca, C., Orlandi, M., Bonano, M., Casu, F., Iesuè, M., Manunta, M., et al. (2024). On the exploitation of the Sentinel-1 P-SBAS service within the EarthConsole® platform for unsupervised on-demand DInSAR processing. In: EGU general assembly 2024; 2024 April 14–19; Vienna, Austria. p. EGU24–EGU15585. doi:10.5194/egusphere-egu24-15585

Dietterich, H. R., Poland, M. P., Schmidt, D. A., Cashman, K. V., Sherrod, D. R., and T, E. A. (2012). Tracking lava flow emplacement on the east rift zone of Kīlauea, Hawai'i, with synthetic aperture radar coherence. *Geochem. Geophys. Geosyst.* 13 (Q05001), 2011GC004016–17. doi:10.1029/2011GC004016

Dzurisin, D., and Lu, Z. (2007). Interferometric synthetic-aperture radar (InSAR). In: *Volcano deformation. Geodetic monitoring techniques*. New York: Springer-Verlag Berlin Heidelberg. p. 153–194.

Eibl, E., Bean, C., Vogfjörd, K., Ying, Y., Lokmer, I., Möllhoff, M., et al. (2017). Tremor-rich shallow dyke formation followed by silent magma flow at bárðarbunga in Iceland. *Nat. Geosci.* 10, 299–304. doi:10.1038/ngeo2906

Elliott, J. R., Biggs, J., Parsons, B., and Wright, T. J. (2008). InSAR slip rate determination on the altyn tagh fault, northern Tibet, in the pres-ence of topographically correlated atmospheric delays. *Geophys. Res. Lett.* 35, L12309. doi:10.1029/2008GL033659

Ellis, A. P., Johanson, I. A., and Poland, M. (2025). Deformation of Mauna Loa before, during, and after its 2022 eruption. *Bull. Volcanol.* 87 (8), 8. doi:10.1007/s00445-024-01788-8

Farr, T. G., Rosen, P., Caro, E., Crippen, R., Duren, R., Hensley, S., et al. (2007). The shuttle radar topography mission. *Rev. Geophys.* 45. doi:10.1029/2005RG000183

Ferretti, A., Prati, C., and Rocca, F. (2001). Permanent scatterers in SAR interferometry. *IEEE Trans. Geoscience Remote Sens.* 39 (1), 8–20. doi:10.1109/36.898661

Field, L., Barnie, T., Blundy, J., Brooker, R. A., Keir, D., Lewi, E., et al. (2012). Integrated field, satellite and petrological observations of the November 2010 eruption of erta ale. *Bullettin Volcanol.* 74, 2251–2271. doi:10.1007/s00445-012-0660-7

Firetto Carlino, M., Lo Bue, R., Taroni, M., Coltelli, M., Cannavò, F., Cocina, O., et al. (2025). Earthquake frequency-magnitude distribution at Mount Etna sheds light on magma ascent in the volcano's plumbing system. *Sci. Adv.* 11, eadx9873. doi:10.1126/sciadv.adx9873

Foubert, A., Keir, D., Atnafu, B., Kidane, T., and the ADD-ON Workshop Consortium (2024). Workshop report: Afar dallol drilling - ONset of sedimentary processes in an active rift basin (ADD-ON). *Sci. Dril.* 33, 207–218. doi:10.5194/sd-33-207-2024

Global Volcanism Program (2023). *Volcanoes of the World (v. 5.0.3; 1 Mar 2023). Distributed by 518 Smithsonian Institution, compiled by Venzke, E.* Washington, DC: Global Volcanism Program. doi:10.5479/si.GVP.VOTW5-2022.5.0

Goldstein, R. M., and Werner, C. L. (1998). Radar interferogram filtering for geophysical applications. *Geophys. Res. Lett.* 25 (21), 4035–4038. doi:10.1029/1998GL900033

Goldstein, R. M., Zebker, H. A., and Werner, C. L. (1988). Satellite radar interferometry: two-dimensional phase unwrapping. *Radio Sci.* 23 (4), 713–720. doi:10.1029/RS023i004p00713

Grandin, R., Jacques, E., Nercessian, A., Ayele, A., Doubre, C., Socquet, A., et al. (2011). Seismicity during lateral dike propagation: insights from new data in the recent manda hararo – Dabbahu rifting episode (afar, Ethiopia). *Geochem. Geophys. Geosyst.* 12 (4), 2010GC003434–24. doi:10.1029/2010GC003434

Hanks, T. C., and Kanamori, H. (1979). A moment magnitude scale. *J. Geophys. Res.* 84 (B5), 2348–2350. doi:10.1029/JB084iB05p02348

Hanssen, R. F. (2001). *Radar interferometry: data interpretation and error analysis*. Netherlands: Kluwer Academic Publishers.

Hensch, M., Dahm, T., Ritter, J., Heimann, S., Schmidt, B., Stange, S., et al. (2019). Deep low-frequency earthquakes reveal ongoing magmatic recharge beneath laacher see volcano (Eifel, Germany). *Geophys. J. Int.* 216 (3), 2025–2036. doi:10.1093/gji/ggy532

Hurman, G. L., Keir, D., Bull, J. M., McNeill, L. C., Booth, A. D., and Bastow, I. D. (2023). Quantitative analysis of faulting in the danakil depression rift of Afar: the importance of faulting in the final stages of magma-rich rifting. *Tectonics* 42, e2022TC007607. doi:10.1029/2022TC007607

Hurman, G. L., Keir, D., McNeill, L. C., Pagli, C., Bull, J. M., and Michas, G. (2025). Seismic and aseismic deformation in the danakil depression, East Africa and corinth rift, Greece: magma-rich vs magma-poor rift extension. *Tectonophysics* 915, 230918. doi:10.1016/j.tecto.2025.230918

Illsley-Kemp, F., Bull, J. M., Keir, D., Gerya, T., Pagli, C., Gernon, T., et al. (2018). Initiation of a proto-transform fault prior to seafloor spreading. *Geochem. Geophys. Geosystems* 19, 4744–4756. doi:10.1029/2018GC007947

Isken, M. P., Karstens, J., Nomikou, P., Parks, M. M., Drouin, V., Rivalta, E., et al. (2025). Volcanic crisis reveals coupled magma system at santorini and Kolumbo. *Nature* 645, 939–945. doi:10.1038/s41586-025-09525-7

Jonsson, S., Zebker, H., Segall, P., and Amelung, F. (2002). Mw7.1 hector mine, California, earthquake, estimated from satellite radar and GPS measurements. *Bull. Seismol. Soc. Am.* 92 (4), 1377–1389. doi:10.1785/0120000922

Kebede, B. A., Pagli, C., Keir, D., Sigmundsson, F., La Rosa, A., Wang, H., et al. (2025). Continuous subsidence of Dallol volcano caused by magmatic, hydrothermal, and salt dissolution processes: insights from InSAR observations. *Geochem. Geophys. Geosyst.* 26, e2024GC012048. doi:10.1029/2024GC012048

Keir, D., La Rosa, A., Raggiunti, M., Wang, H., Ayele, A., Lewi, E., et al. (2025). The 2024 fentale diking episode in a slow extending Continental rift. *Geophys. Res. Lett.* 52, e2024GL113214. doi:10.1029/2024GL113214

La Rosa, A., Pagli, C., Keir, D., Sani, F., Corti, G., Wang, H., et al. (2019). Observing oblique slip during rift linkage in northern Afar. *Geophys. Res. Lett.* 46, 10782–10790. doi:10.1029/2019GL084801

La Rosa, A., Pagli, C., Hurman, G. L., and Keir, D. (2022). Strain accommodation by intrusion and faulting in a rift linkage zone: evidences from high-resolution topography data of the afrera plain (Afar, East Africa). *Tectonics* 41, e2021TC007115. doi:10.1029/2021TC007115

La Rosa, A., Raggiunti, M., Pagli, C., Keir, D., Wang, H., and Ayele, A. (2023). Extensional earthquakes in the absence of magma in Northern Afar: insights from InSAR. *Geophys. Res. Lett.* 50, e2023GL102826–9. doi:10.1029/2023GL102826

La Rosa, A., Pagli, C., Wang, H., Sigmundsson, F., Pinel, V., and Keir, D. (2024). Simultaneous rift-scale inflation of a deep crustal sill network in Afar, East Africa. *Nat. Commun.* 15, 4287. doi:10.1038/s41467-024-47136-4

Lanari, R., Casu, F., Manzo, M., Zeni, G., Berardino, P. M. M., Pepe, A., et al. (2007). An overview of the small BAseline subset algorithm: a DInSAR technique for surface deformation analysis. *Pure Appl. Geophys.* 164, 637–661. doi:10.1007/978-3-7643-8417-3_2

Maccaferri, F., Rivalta, E., Passarelli, L., and Aoki, Y. (2016). On the mechanisms governing dike arrest: insight from the 2000 miyakejima dike injection. *Earth Planet. Sci. Lett.* 434, 64–74. doi:10.1016/j.epsl.2015.11.024

Makris, J., and Ginzburg, A. (1987). The Afar depression: transition between continental rifting and sea-floor spreading. *Tectonophysics* 141 (1-3), 199–214. doi:10.1016/0040-1951(87)90186-7

Moore, C., Wright, T. J., Hooper, A., and Biggs, J. (2019). The 2017 eruption of erta 'ale Volcano, Ethiopia: insights into the shallow axial plumbing system of an incipient Mid-ocean Ridge. *Geochem. Geophys. Geosyst.* 20, 5727–5743. doi:10.1029/2019GC008692

Naranjo, C., Euillades, C. P., Toyos, D. G., Euillades, C. L., and Villarosa, B. G. (2022). Application of a temporal decorrelation model using Sentinel-1 SAR data to detect volcanic ash deposits related to the 2020 taal volcano eruption. *Remote Sens. Appl. Soc. Environ.* 31, 100991. doi:10.1016/j.rsase.2023.100991

Nikkhoo, M., Walter, T. R., Lundgren, P. R., and Prats-Iraola, P. (2017). Compound dislocation models (CDMs) for volcano deformation analyses. *Geophys. J. Int.* 208 (2), 877–894. doi:10.1093/gji/ggw427

Nobile, A., Pagli, C., Keir, D., Wright, T. J., Ayele, A., Ruch, J., et al. (2012). Dike-fault interaction during the 2004 dallol intrusion at the northern edge of the erta ale ridge (afar, Ethiopia). *Geophys. Res. Lett.* 39 (L19305), 2012GL053152–7. doi:10.1029/2012GL053152

Okada, Y. (1985). Surface deformation due to shear and tensile faults in a half-space. *Bull. - Seismol. Soc. Am.* 75 (4), 1135–1154. doi:10.1785/bssa0750041135

Pagli, C., Wright, T. J., Ebinger, C. J., Yun, S., Cann, J. R., Barnie, T., et al. (2012). Shallow axial magma chamber at the slow-spreading erta ale ridge. *Nat. Geosci.* 5 (4), 284–288. doi:10.1038/ngeo1414

Pallister, J., McCausland, W., Jónsson, S., Lu, Z., Zahran, H. M., El Hadidy, S., et al. (2010). Broad accommodation of rift-related extension recorded by dyke intrusion in Saudi Arabia. *Nat. Geosci.* 3, 705–712. doi:10.1038/ngeo966

Parks, M., Drouin, V., Sigmundsson, F., Hjartardóttir, Á. R., Geirsson, H., Pedersen, G. B., et al. (2025). 2023–2024 inflation-deflation cycles at svartsengi and repeated dike injections and eruptions at the sundhnúkur crater row, Reykjanes peninsula, Iceland. *Earth Planet. Sci. Lett.* 658, 119324. doi:10.1016/j.epsl.2025.119324

Peng, L., Wang, H., Ng, A. H.-M., and Yang, X. (2022). SAR offset tracking based on feature points. *Front. Earth Sci.* 9, 724965. doi:10.3389/feart.2021.724965

Pin, J., Chazot, G., France, L., Abily, B., Gurenko, A., Bertrand, H., et al. (2024). Protracted magma evolution and transcrustal magmatic plumbing system architecture at erta ale volcano (Afar, Ethiopia). *J. Petrology* 65 (65), egae118. doi:10.1093/petrology/egae118

Remie, M., Avouac, J., and Taboury, J. (1999). Measuring ground displacements from SAR amplitude images: application to the Landers earthquake. *Geophys. Res. Lett.* 26 (7), 875–878. doi:10.1029/1999GL900138

Richter, C. F. (1935). An instrumental earthquake magnitude scale. *Bull. Seismological Society Am.* 25 (1), 1–32. doi:10.1785/bssa0250010001

Rime, V., Negga, H., Fentimen, R., Rüggeberg, A., El Korh, A., Pirkenseer, C., et al. (2025). Nature and significance of late Pleistocene to Holocene thick evaporite deposits of the Danakil depression, Afar, Ethiopia. *Sedimentology* 72 (2), 475–506. doi:10.1111/sed.13237

Rivalta, E., Corbi, F., Passarelli, L., Acocella, V., Davis, T., and Di Vito, M. A. (2019). Stress inversions to forecast magma pathways and eruptive vent location. *Sci. Adv.* 5 (7), eaau9784. doi:10.1126/sciadv.aau9784

Rivalta, E., and Segall, P. (2008). Magma compressibility and the missing source for some dike intrusions. *Geophys. Res. Lett.* 35, L04306. doi:10.1029/2007GL032521

Rosen, P. A., Gurrola, E. M., Sacco, G. F., and Zebker, H. (2012). The InSAR scientific computing environment. In: EUSAR 2012; 9th European conference on synthetic aperture radar: IEEE. p. 730–733.

Sigmundsson, F., Hooper, A., Hreinsdóttir, S., Vogfjörd, K. S., Ófeigsson, B. G., Heimisson, E. R., et al. (2015). Segmented lateral dyke growth in a rifting event at bárðarbunga volcanic system, Iceland. *Nature* 517, 191–195. doi:10.1038/nature14111

Sigmundsson, F., Parks, M., Geirsson, H., Hooper, A., Drouin, V., Vogfjörd, K. S., et al. (2024). Fracturing and tectonic stress drive ultrarapid magma flow into dikes. *Science* 283 (6688), 1228–1235. doi:10.1126/science.adn2838

Simons, M., Fialko, Y., and Rivera, L. (2002). Coseismic deformation from the 1999 Mw 7.1 hector mine, California, earthquake as inferred from InSAR and GPS observations. *Bull. Seismol. Soc. Am.* 92 (4), 1390–1402. doi:10.1785/0120000933

Varugu, B., and Amelung, F. (2021). Southward growth of mauna Loa's dike-like magma body driven by topographic stress. *Sci. Rep.* 11 (9816), 9816. doi:10.1038/s41598-021-89203-6

Viltres, R., Jonsson, S., Ruch, J., Doubre, C., Reilinger, R., Floyd, M., et al. (2020). Kinematics and deformation of the southern Red Sea region from GPS observations. *Geophys. J. Int.* 221, 2143–2154. doi:10.1093/gji/ggaa109

Watts, E., Gernon, T. M., Taylor, R. N., Keir, D., and Pagli, C. (2023). Magmatic evolution during proto-oceanic rifting at alu, dalafilla and borale volcanoes (Afar) determined by trace element and sr-nd-pb isotope geochemistry. *Lithos* 456-457, 107311–107457. doi:10.1016/j.lithos.2023.107311

Wieser, P. E., Shi, S. C., Gleeson, M. L. M., Rangel, B., DeVitre, C. L., Bearden, A. T., et al. (2025). Fluid inclusion constraints on the geometry of the magmatic plumbing system beneath Mauna Loa — part 1: Lavas and tephras. *Bull. Volcanol.* 87 (89), 89. doi:10.1007/s00445-025-01874-5

Wright, T. J., Ebinger, C., Biggs, J., Ayele, A., Yirgu, G., Keir, D., et al. (2006). Magma-maintained rift segmentation at continental rupture in the 2005 Afar dyking episode. *Nature* 442 (7100), 291–294. doi:10.1038/nature04978

Wright, T., and Pilger, E. (2008). Radiant flux from Earth's subaerially erupting volcanoes. *Int. J. Remote Sens.* 29, 6443–6466. doi:10.1080/01431160802168210

Wright, T., Sigmundsson, F., Pagli, C., Belachew, M., Hamling, I. J., Brandsdottir, B., et al. (2012). Geophysical constraints on the dynamics of spreading centres from rifting episodes on land. *Nat. Geosci.* 5, 242–250. doi:10.1038/ngeo1428

Xu, W., Rivalta, E., and Li, X. (2017). Magmatic architecture within a rift segment: articulate axial magma storage at erta ale volcano, Ethiopia. *Earth Planet. Sci. Lett.* 476, 79–86. doi:10.1016/j.epsl.2017.07.051

Xu, W., Xie, L., Aoki, Y., Rivalta, E., and Jonsson, S. (2020). Volcano - wide deformation after the 2017 erta ale dike intrusion, Ethiopia, observed with radar interferometry journal of geophysical research: solid Earth. *J. Geophys. Res. Solid Earth* 125, e2020JB019562. doi:10.1029/2020JB019562